In situ, non-covalent labeling and super-resolution STED imaging of supramolecular peptide nanostructures

Mohit Kumar, [*, †] *Jiye Son,*[†] *Hailin Huang,*[†, ξ, ‡] *Deborah Sementa,*[†] *Magdelene Lee,*[†] *Stephen O'Brien,*[†, ξ, ‡] *and Rein V. Ulijn*[*, †, ‡, §]

[†]Advanced Science Research Center (ASRC) at The Graduate Center, City University of New York, 85 St. Nicholas Terrace, New York, NY 10031, USA; [‡]PhD Program in Chemistry, The Graduate Center, CUNY, 365 Fifth Avenue, New York, NY 10016, USA; [§]Department of Chemistry, Hunter College, CUNY, 695 Park Avenue, New York, NY 10065, USA; [ξ]Department of Chemistry and Biochemistry, The City College of New York, 1024 Marshak, 160 Convent Avenue, New York, NY 10031, USA.

ABSTRACT: Supramolecular materials have gained substantial interest for a number biological and non-biological applications. However, for optimum utilization of these dynamic self-assembled materials, it is essential to visualize and understand their structures at the nanoscale, in solution and in real-time. Previous approaches for imaging these structures have utilized super-resolution optical imaging methods like STORM which require complicated and multi-step sample preparation with slow acquisition times which limits real-time *in situ* imaging of dynamic processes. We demonstrate a non-covalent fluorescent labeling design for STED based super-

resolution imaging of self-assembling peptides. This is achieved by *in situ*, electrostatic binding of anionic sulfonates of Alexa-488 dye to the cationic sites of lysines and arginines exposed on the peptide nanostructure surface. A direct, multiscale visualization of these structures reveals hierarchical organization of supramolecular fibers with sub 60 nm resolution. In addition, dynamic dis-assembly of nanofibers upon enzymatic hydrolysis of peptide could be directly imaged in real-time to provided mechanistic insights into the process. Labelling of a range of cationic self-assembling peptides and peptide-functionalized gold nanoparticles demonstrated the versatility of the methodology for the labelling of cationic supramolecular structures. Overall, this presents a general and simple design of electrostatic fluorescent labeling of cationic peptide nanostructures for nanoscale imaging under physiological conditions and probe dynamic processes in real-time and *in situ*.

KEYWORDS: super-resolution imaging, peptide nanostructures, STED optical microscopy, dynamic self-assembly, electrostatic fluorescent labeling, real-time imaging.

Self-assembly of small molecules through non-covalent interactions is a powerful strategy to produce synthetic materials with novel functions.[1-4] Short peptides represent a particularly versatile class of supramolecular materials,[5] with a wide range of applications in nanotechnology[6] and biomedicine.[7] These structures often display hierarchical organization, and in order to understand and predict their properties and functions it is essential to understand the organization across the length scales, from molecular to nano, micro, and macro.[6] In addition, dynamic aspects are increasingly investigated, including morphological reconfiguration,[8-11] transient and active self-assembly,[12-17] analysis of dynamic interactions with cells,[18] formation of intracellular filaments[19] or growth dynamics of amyloid like peptide self-assembly.[20] *In situ* imaging of these

dynamic nanostructures has mainly relied on diffraction-limited (by the Abbe limit, >200 nm) fluorescence (confocal) microscopy.[12, 21-23] In addition, recent developments enable dynamic imaging at the nanoscale, using *e.g.* liquid cell transmission electron microscopy (TEM)[24-25] and liquid cell atomic force microscopy (AFM).[26]

Super-resolution optical microscopy (SRM) is an effective method to image biological samples with resolution beyond the diffraction limit,[27] and is increasingly used outside biology to study the morphology and dynamic behavior of nanoscale supramolecular systems. The first report of SRM on the dynamic self-assembly of small molecules by Meijer *et al*. utilized stochastic optical reconstruction microscopy (STORM) to quantitatively probe the molecular exchange in dynamic nanofibers with ~25 nm spatial resolution.[28] STORM and other SRM techniques have also been used to investigate supramolecular polymerization of various peptide amphiphiles which provided insights like the presence of segments with varying dynamicity within the same fibers *etc*.[29-31] While STORM provides unmatchable spatial resolution, it is slow and requires additional sample treatment, which limits the scope for direct observation of dynamic processes in their native environment. Stimulated emission-depletion (STED) microscopy,[32-35] holds promise for *in situ* real-time imaging of dynamic nanostructures, as demonstrated by Hamachi *et al.* in visualizing self-sorted hydrogel network of peptide and amphiphilic phosphate.[36] These examples demonstrated breakthroughs in nanoscale imaging of self-assembly, however, they require covalent conjugation of a fluorophore onto the self-assembling unit, which adds additional steps to the synthesis and purification procedure and can adversely influence the self-assembly process.[37]

We introduce a general method for *in situ* SRM imaging of self-assembling peptide nanostructures using a non-covalent labeling approach with a dye that is compatible with STED

imaging. We demonstrate that the non-covalent dye labeling design requires only low levels of labeling (0.5 mole%) which does not interfere with the self-assembly and circumvents the tedious covalent labeling process. Furthermore, the STED microscopy enables super-resolution imaging and elucidation of hierarchical organization of peptide nanofibers under physiological conditions (Figure 1), as well as *in situ* and real-time imaging of enzymatic breakdown of these fibers.

RESULTS AND DISCUSSION

Rational design of non-covalent labeling. Our fluorescent labeling approach utilizes the non-specific electrostatic interactions between positively charged amines present on the surface of self-assembled peptides and the negatively charged sulfonates of the Alexa-488 dye (Figure 1). Previous reports on amine-sulfonate interactions have been utilized to quantify amines on surfaces,[38] and for spatially controlled gelation of sulfonated azo dye on cationic surface.[39] Alexa-488 dye contains two negatively charged sulfonates (Figure 1) and hence displays strong interactions with amines. Indeed, we recently reported that enzyme functionalized with Alexa-488 could be used to immobilize and visualize enzymes onto nanopatterned amine surfaces.[40-41] Conveniently, Alexa-488 is also a known dye for STED imaging.[42] Thus, we envisaged that it can be used for non-covalent fluorescent labeling of positively charged peptide nanostructures for super-resolution imaging. Although non-covalent fluorescent labeling has been reported for confocal fluorescent imaging of nanostructures,[43-44] our report of electrostatic dye labeling presents a unique example for super-resolution imaging.

We chose decapeptide **1** (FFALGLAGKK) as a model amphiphilic peptide which contains a self-assembling sequence derived from the well-known FF dyad,[45] an enzyme cleavable middle

section, and a hydrophilic C-terminus containing two positively charged lysine (K) residues. The peptide was previously reported to self-assemble into nanofibers and imaged using AFM.[8]

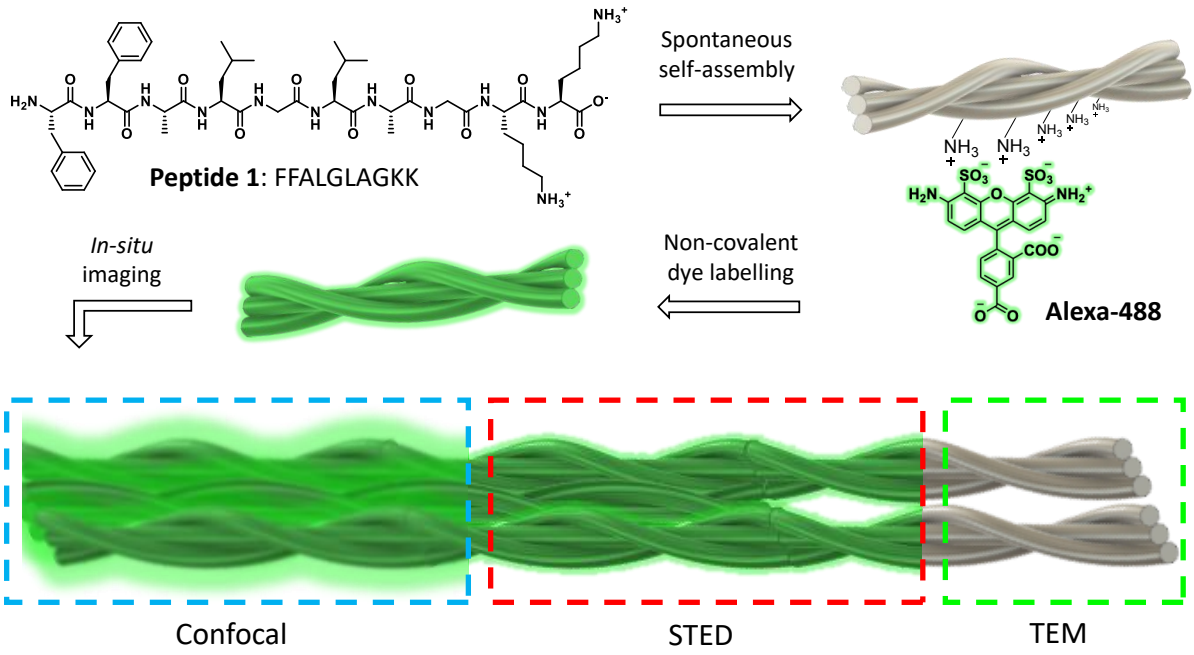

Figure 1. Schematic showing non-covalent Alexa-488 labeling of peptide **1** nanostructure for STED SRM imaging.

Super-resolution imaging with STED. Self-assembly of **1** was investigated at physiological conditions (5 mM in aqueous phosphate buffer, pH 7.4) using confocal laser scanning microscopy (CLSM). Fluorescent labeling was performed by mixing Alexa-488 dye (0.5 mole % of **1**) with a solution containing preformed nanostructures. CLSM imaging revealed the formation of a network of nanofibers, and individual fiber bundles, albeit with diffraction limited resolution (Figures 2a-b). When the same area was imaged in STED mode, a significant enhancement in the resolution was observed (Figures 2c-d, Figure S1-2). To graphically present the difference in resolution between STED and CLSM, we plotted the fluorescence intensity profile through the center of the

box shown in Figure 2b, 2d. As evident from Figure 2e, STED can clearly resolve two individual fiber bundles which were otherwise imaged as a single structure using traditional CLSM.

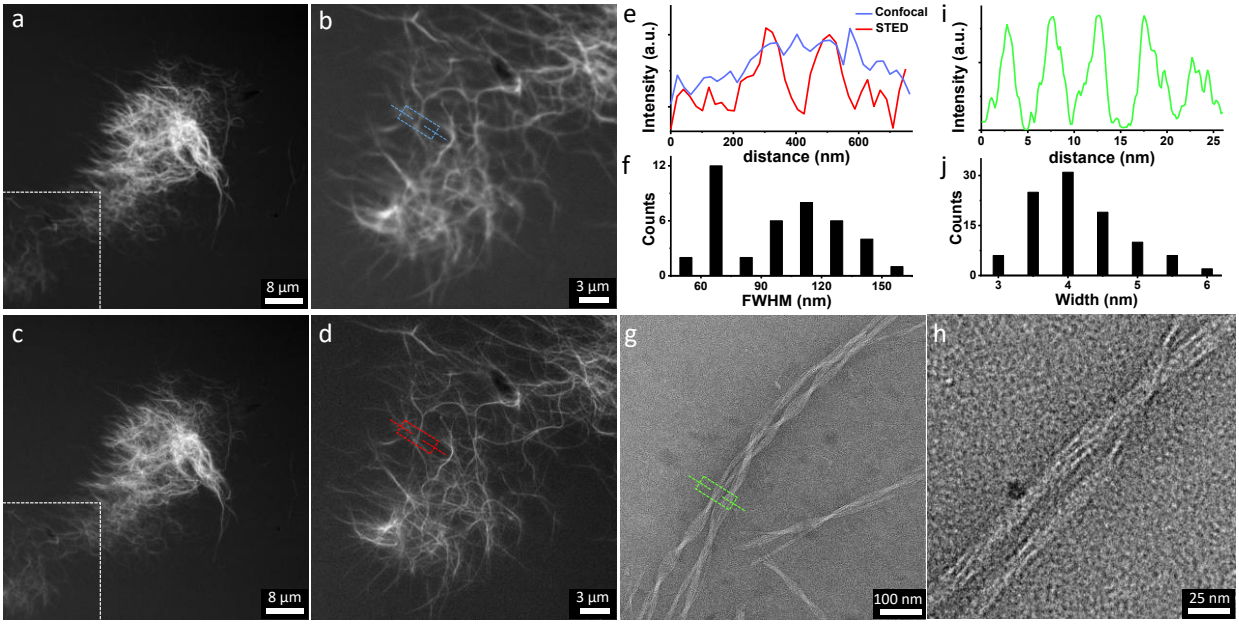

Figure 2. Fluorescence imaging with super-resolution: Comparative CLSM (a-b) and STED (c-d) micrographs of self-assembled **1** (5 mM in aqueous phosphate buffer, pH=7.4) labeled with 0.5 mole % Alexa-488. e) Comparison of fluorescence intensity profile plotted through the center of the box shown in b) and d) demonstrate the advantage of STED to resolve individual fibers compared to CLSM. f) Histogram showing the bimodal distribution of fiber width measured as FWHM (from STED images of 40 fibers). TEM micrograph (g-h) displaying hierarchical organization. i) Intensity profile along the center of green box shown in g) demonstrate fiber bundle formation whereas j) shows the fiber width distribution (from TEM image of 100 fibers).

To determine the limit of resolution, full width at half maxima (FWHM) was obtained from the fluorescence intensity profile across individual nanostructures. A histogram plot of FWHM showed a bimodal distribution with peak maxima around 65 nm and 115 nm (Figure 2f, Figures

S1-S3), indicating formation of intertwined super-structures. Furthermore, we could observe individual nanostructures down to 52 nm (Figure S3).[36] A comparison of FWHM analysis of nanofibers confirm the enhanced resolution of STED compared to CLSM (Figure S1).

The data in Figure 2f indicate a hierarchical organization as schematically shown in Figure 1, which was further confirmed by TEM analysis. TEM showed the formation of individual one-dimensional fibrils with width around 4 nm (Figure 2 g-j, Figure S4), where approximately 3 to 8 of them align and the resulting tapes twist around each other to form super-structures. The complementarity of STED imaging is clearly useful to gain a complete picture of hierarchical organization of these fibers, and it also addresses issues regarding drying artifacts in dry state TEM. STED SRM provides the crucial nanostructure information in solution in the 50-200 nm window, which can enable a more seamless connection between different imaging techniques.

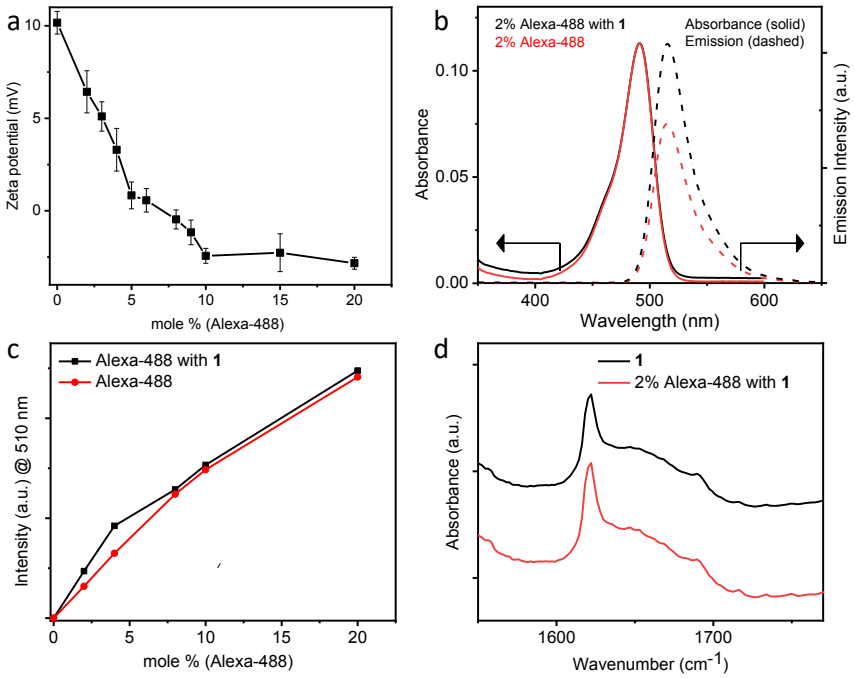

Figure 3. Non-covalent fluorescence labeling: a) Variation in zeta potential of **1** upon addition of aliquots of Alexa-488 dye. b) Absorption (solid lines) and emission (dashed lines) spectral

changes of **1** with (black) and without (red) 2% of Alexa-488 dye showing enhanced emission upon peptide-dye interaction which is advantageous for fluorescent imaging. c) Comparative plot showing difference in fluorescence intensity of Alexa 488 at 510 nm with and without **1** peptide. d) FTIR spectra in the amide-I region showing antiparallel β-sheet hydrogen bonding of the peptide backbone which is unaffected upon dye labeling.

Characterization of fluorescent labeling process. When using a non-covalent electrostatic labelling approach, care should be taken not to disrupt the electrostatics of the system. Thus, to gain insights into the mode of the labeling process and interaction between the dye and the nanostructure, zeta potential was measured in the presence of variable concentrations of dye. A titration of **1** with Alexa-488 shows that the positively charged surface of self-assembled **1** (zeta potential of 10.2 mV) becomes near-neutral (0.83 mV) upon addition of 5 % of Alexa-488 which then turns negative (-2.4 mV) and plateaus beyond 10 % (Figure 3a). These observations confirm the electrostatic interaction of the dye with the positively charged lysines present on the nanostructure surface. UV-Vis absorption and fluorescence spectra of Alexa-488 remain largely unaffected by the interaction with the peptide, with a modest enhancement in emission intensity observed at 515 nm (Figure 3b, Figure S5). A comparative plot of fluorescence intensity of the dye in the absence or presence of peptide nanostructure shows an initial increase in emission of dye (by 42%) in the presence of **1** up to 4 mole % of dye, before it becomes similar to dye alone beyond 10 mole% (Figure 3c), in line with the trend in Figure 3a. We propose that the increase in emission at lower dye loading could be due to enhanced physical separation between dye molecules which is a result of anchoring onto the fiber surface, whereas higher dye % could induce inter-dye interactions. Fourier transform infrared (FTIR) spectroscopic analysis further shows that the anti-parallel β-sheet structure of **1** remains unaffected upon dye labeling (Figure 3d), ruling out

any nanostructure artifacts in presence of the dye. Furthermore, TEM imaging of self-assembled **1** with and without dye show that nanofibers remain unaffected (Figure S6). Thus, we have demonstrated that simple electrostatic interaction between Alexa-488 and peptide can be effectively used for SRM imaging without any undesirable effects on assembly.

Having demonstrated the non-specific electrostatic interactions between the negatively charged sulfonate of Alexa-488 and positively charged lysines of peptides, we investigated the generality of the approach with a number of additional positively charged nanostructures. Thus, we studied the Alexa-488 labeling of **2**, which is similar to **1** except that alanine (A3) is replaced by proline (P). **2** is also known to form nanofibers[8] with the positively charged lysines (zeta potential 15.4 mV) on the surface and could be visualized with STED SRM (Table 1, Figure S7). Furthermore, we investigated if other positively charged amino acids like arginine (R) containing peptide nanostructures could be labeled with our design. Thus, we investigated the self-assembly of peptide **3**, which is analogous to **1** where positive charge is provided by arginine (R) instead of lysine (K). We observe the formation of one-dimensional nanofibers which could also be labeled by Alexa-488 (Figure S8). Interestingly, STED imaging of these nanostructures demonstrated the formation of fluorescent nanofibers in solution. Thus, we have demonstrated the versatility of our alexa-488 based electrostatic fluorescent labeling of a broad class of positively charged peptides containing lysines and arginines.

To further confirm our hypothesis, we observed that Alexa-488 could not label negatively charged peptide nanostructures **7** (zeta potential -34.9 mV), containing anionic aspartic acid (D) instead of lysine (K) on peptide surface, due to electrostatic repulsion with negatively charged sulfonate groups of Alexa-488. Furthermore, there is a clear zeta potential cut-off such that charged nanostructures **4**, **5, 6** (zeta potential 8.2 mV, 4.1 mV, 1.3 mV, respectively) could not be imaged

through Alexa-488 staining (Figure S9), indicating that the nanostructure surface needs to have sufficient positive charge to enable anchoring of the dye for STED SRM.

Table 1. Different peptide nanostructures and peptide functionalized gold nanoparticles investigated along with their corresponding amino acid sequences, zeta potential value and the suitability for STED SRM imaging.

Nanostructures	Sequence	Zeta potential (mV)	Dye labeling for STED SRM imaging
1	FFALGLAGKK	11.5	Yes
2	FFPLGLAGKK	15.4	Yes
3	FFALGLAGRR	10.3	Yes
Au-1K	KPKGLRGDC-Au	18.1	Yes
Au-2K	KKPKGLRGDC-Au	24.6	Yes
Au-3K	KKKPKGLRGDC-Au	28.7	Yes
4	FFGALGLKGK	8.2	No
5	FFGPLGLKGK	4.1	No
6	FFGAAGLKGK	1.3	No
7	FFALGLAGDD	-34.9	No

To demonstrate the general utility of our approach we tested gold nanoparticles functionalized with cationic peptide ligands, as a model system for therapeutic and diagnostic applications.[46] We synthesized **Au-1K**, **Au-2K** and **Au-3K** (zeta potential 18.1 mV, 24.6 mV, 28.7 mV respectively) containing increasing numbers of positively charged lysines. Interestingly, all of them could be visualized by our design of electrostatic labeling with Alexa-488 (Table 1, Figure S10-12). We observed that the resolution of STED imaging was not very high for gold nanoparticles which could be due to partial quenching of the dye. It should be noted that fluorescence imaging of peptides attached to gold nanoparticles is not trivial due to the general tendency of gold nanoparticles to quench the emission of fluorophore covalently conjugated on its surface.[47]

Previous report have shown that indirect fluorescence labeling on metal nanoparticles can significantly reduce the fluorescence quenching.[48] Advantageously, our electrostatic labeling design enables imaging of peptide conjugated gold nanoparticles without completely quenching of emission. Thus, we have demonstrated the modular nature of Alexa-488 labeling design which can be used for fluorescent imaging of gold nanoparticles conjugated with cationic peptides.

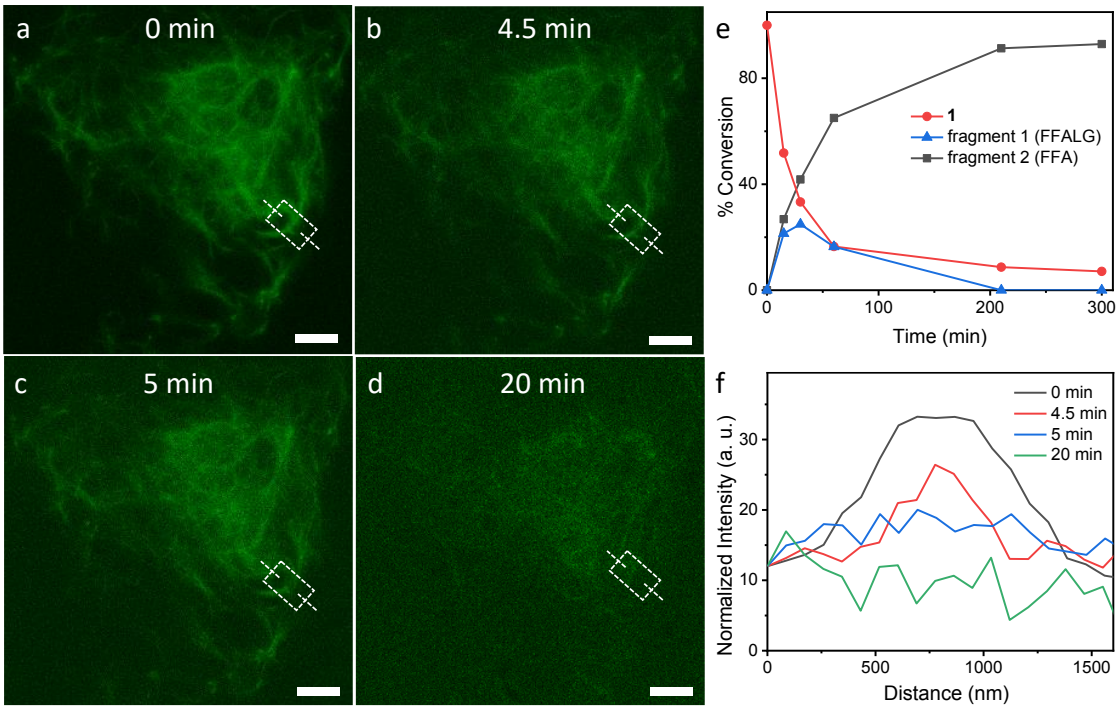

Figure 4. Real-time imaging of fiber disintegration: (a-d) Snapshots of real-time and *in situ* STED imaging of **1** in presence of thermolysin at pH 7.4, resulting in disintegration of nanofibers over time (scale bar = 3 μm). e) Time dependent HPLC profile of hydrolysis of peptide **1** (5 mM at pH 7.4) in presence of 0.005 mg/ml of thermolysin. f) Plot of normalized fluorescence intensity profile through the center of the white box at different time points. The results demonstrate that the enzyme act directly on the self-assembled fiber surface, as seen particularly in the boxed area. The observed kinetic discrepancy between STED imaging (a-d) and HPLC analysis (e) relates to

the fact that STED probes the existence of supramolecular fibers in the focal plane while HPLC analysis reveals the overall peptide hydrolysis in the bulk.

Real-time visualization of dynamic disassembly. Finally, we demonstrate the versatility of our strategy for *in situ* imaging of an enzymatic dis-assembly process in real-time. Peptide **1** was designed to be hydrolyzed by matrix metalloproteinases.[8] However, this proteolytic process is slow (occurs in days), so an alternative enzyme was selected. So, we demonstrate disintegration of Alexa-488 labeled peptide **1** using the metalloprotease, thermolysin, as a model enzyme. We observed rapid digestion over a period of 50 minutes (as monitored by HPLC), which is more amenable to *in situ* and real time imaging. Two major products of thermolysin catalyzed hydrolysis (Fragment 1 and 2, Figure 4e, Figure S13) losses lysine and the amphiphilicity for self-assembly. Snapshots at various time points show that the nanofibers were gradually broken down while an enhancement of background fluorescence was simultaneously observed, due to increase in released free dye in solution (Figure 4 a-d and Video S1). Interestingly, by focusing on the boxed region of the fiber, it is evident that the nanostructures thin out from the interior of the fiber, not the edges (fluorescence profile, Figure 4f), before it fragments. This analysis confirms that thermolysin can directly act on the self-assembled nanostructure, ruling out the exclusive action of thermolysin on the monomeric peptides in solution to drive dis-assembly. Thus, we have demonstrated that our non-covalent labeling method combined with STED can provide mechanistic insight into enzymatic action and propose that the methodology can provide crucial information to previous work on enzymatic assembly/disassembly of peptides. We note that the spatial resolution in the real-time image was lower than the static images in Figure 2 due to faster scan rate as multiple images were collected over long duration and the large sample depth for enzymatic reaction. Moreover, SRM imaging of enzyme responsive assemblies have been previously reported with

STORM, however samples required covalent labeling and imaging only in special imaging solution at various time points instead of live imaging.[30, 49]

CONCLUSIONS

In conclusion, we have presented a general strategy for super-resolution fluorescent imaging of cationic peptide nanostructures. By using electrostatic interaction between cationic groups on the nanostructure surface and sulfonate groups in Alexa-488 dye, a range of lysine and arginine containing nanofibers could be effectively imaged. These nanostructures were visualized by STED based super-resolution microscopy with resolution down to 52 nm. By changing the peptide structure, we could vary the zeta potential of the supramolecular surfaces, as well as peptide-functionalized gold nanoparticles. We observed that nanostructures which were sufficiently positively charged (zeta potential >10 mV) could be imaged with STED SRM. Additionally, a dynamic process, exemplified by enzymatic disintegration of a peptide nanostructure could be visualized in real-time and *in situ*. This simple and general strategy for super-resolution imaging of dynamic soft nanostructures in their native aqueous environment can be used to investigate bio-inspired active assembly.[12] Furthermore, since Alexa-488 co-assembly with peptides has been utilized for enhanced cellular permeability of the dye,[50] our design of non-covalent conjugation combined with SRM opens the door for *in vivo* imaging and for probing biochemical processes using supramolecular materials for bio-medical applications.

EXPERIMENTAL METHODS

Confocal laser scanning microscopy (CLSM) and Stimulated emission depletion (STED) microscopy (SRM). CLSM and STED imaging were performed using Leica TCS SP8 STED 3X with 100x objective lens (with oil immersion). White Light Laser (470-670 nm) was used to excite

the fluorophore with 488 nm source (12 % intensity with 70% output laser power) and emission was collected at 500 nm – 580 nm window. STED depletion was performed using 592 nm depletion laser (21 % intensity with 80 % output laser power). For imaging, scan speed was 200 hz, with 4 line average and 2 frame accumulation and pixel size of 13 nm x 13 nm (2048 x 2048 scan) in the xy plane. The HyD detector was used for collecting emission in 500 nm – 580 nm window with gating from 0.3 ns to 6 ns to filter excitation laser.

Sample preparation. 50 µl of self-assembled **1** solution (5 mM of **1** in 10 mM aqueous phosphate buffer, pH=7.4 at room temperature) was taken in a vial and 10 mM aqueous stock solution of Alexa-488 dye was added such that the final concentration of the dye was 25 µM (*i.e.* 0.5 mole % of **1**). The solution was allowed to mix in a shaker bath for 30 min before imaging. 15 µl of the above solution was placed between a glass slide and a cover slip (0.15–0.18 mm thickness) and sealed with transparent nail polish.

For dynamic real-time imaging (Figure 5 and supporting video video), 30 to 40 µl of the above solution was spotted on a glass-bottomed petri dish closed with a lid (non-coat, 0.15–0.18 mm glass bottom thickness) and incubated with water drops around the sample (to avoid sample drying) at room temperature. This was placed on the microscope and a suitable area was brought into focus for imaging. To this solution thermolysin was added and sample was continuously imaged every 30 sec for 1 hr till enzymatic reaction was completed.

Zeta-Potential. The zeta (ζ)-potential measurements were made on Anton Paar Litesizer 500 Particle Analyzer. Peptide samples (5 mM) were prepared in 2% PBS, and the pH was adjusted to 7.4 using dilute NaOH and HCl. Fifty microliters of the sample was pipetted into Univette low volume cuvette, and three series of measurements were made at 25 °C using Smoluchowski

approximation. Similar measurements were performed by adding aliquots of Alexa-488 stock solution to the required concentration.

Solid-Phase Peptide Synthesis. Peptides were synthesized on CEM Liberty Blue microwave-assisted solid-phase peptide synthesizer using ~1:5 resin to amino acid ratio and excess diisopropylcarbodiimide, Oxyma (ethyl(hydroxyimino)cyanoacetate), and 20% piperidine in dimethylformamide. The desirable peptide-loaded resins were washed three times in dichloromethane, followed by three washes in diethyl ether on a filtration column. The peptides were cleaved from the resins, and side chain protecting groups were removed by reacting with a solution containing 95% trifluoroacetic acid, 2.5% triisopropyl silane, and 2.5% water for 2 h. The cleaved peptides were recovered by removing the TFA, followed by precipitation in cold diethyl ether. Peptides were washed three times in cold diethyl ether and centrifuged to decant the supernatant. The crude peptides were dissolved in Milli-Q water, lyophilized and purified on preparative reverse phase high pressure liquid chromatography (HPLC).

Transmission Electron microscopy (TEM). The TEM images were taken on FEI Titan Themis 200kV TEM (USA). Peptide solution (1 mM) was prepared in 10 mM phosphate buffer (pH 7.4) sonicated for 10 min, and 5 μL of the solution was drop casted on a carbon film grid (400 mesh, copper) and dried completely. To the dry grid was added 5 μL of Milli-Q water and quickly blotted to wash away the phosphate salts and dried completely. Finally, 5 μL of methylamine vanadate-based negative stain (NanoVan by Nanoprobes) was drop casted, blotted away, and dried completely.

ASSOCIATED CONTENT

Supporting Information. Synthesis, additional materials and methods and supporting data is available free of charge on the ACS Publications website.

The following files are available free of charge.

Materials and methods, synthesis and supporting figures (file type: PDF)

real-time nanostructure disintegration video (file type: video)

AUTHOR INFORMATION

Corresponding Author

*Email: mkumar@gc.cuny.edu, rulijn@gc.cuny.edu

Notes

The authors declare no competing financial interests.

ACKNOWLEDGMENT

The authors acknowledge the staff of imaging suite facility at Advanced Science Research Center (ASRC) for STED SRM, Heeyeun Shon for the schematic design in Figure 1, Dhwanit Dave for useful discussions, funding from the US Air Force Office of Scientific Research (grant number FA9550-15-1-0357), US-Israel Binational Science Foundation (grant number 2017510), US Army Research Laboratory and US Army Research Office (grant number W911NF-16-1-0113). We thank the NSF CREST Center for Interface Design and Engineered Assembly of Low Dimensional Systems (IDEALS) (NSF grant number HRD-1547830), the NSF REU site: Nano-NY (award numbers 1659629 and 1659808), NSF DMR-1461499 and NSF CHE-1808143.

REFERENCES

1. Aida, T.; Meijer, E. W.; Stupp, S. I., Functional Supramolecular Polymers. *Science* **2012,** *335*, 813-817.

2. Du, X.; Zhou, J.; Shi, J.; Xu, B., Supramolecular Hydrogelators and Hydrogels: From Soft Matter to Molecular Biomaterials. *Chem. Rev.* **2015,** *115*, 13165-13307.
3. Webber, M. J.; Appel, E. A.; Meijer, E. W.; Langer, R., Supramolecular biomaterials. *Nat. Mater.* **2016,** *15*, 13-26.
4. Chivers, P. R. A.; Smith, D. K., Shaping and structuring supramolecular gels. *Nat. Rev. Mater.* **2019,** *4*, 463-478.
5. Zhang, S., Fabrication of novel biomaterials through molecular self-assembly. *Nat. Biotechnol.* **2003,** *21*, 1171.
6. Yuan, C.; Ji, W.; Xing, R.; Li, J.; Gazit, E.; Yan, X., Hierarchically oriented organization in supramolecular peptide crystals. *Nat. Rev. Chem.* **2019,** *3*, 567-588.
7. Cheetham, A. G.; Chakroun, R. W.; Ma, W.; Cui, H., Self-assembling prodrugs. *Chem. Soc. Rev.* **2017,** *46*, 6638-6663.
8. Son, J.; Kalafatovic, D.; Kumar, M.; Yoo, B.; Cornejo, M. A.; Contel, M.; Ulijn, R. V., Customizing Morphology, Size, and Response Kinetics of Matrix Metalloproteinase-Responsive Nanostructures by Systematic Peptide Design. *ACS Nano* **2019,** *13*, 1555-1562.
9. Inostroza-Brito, K. E.; Collin, E.; Siton-Mendelson, O.; Smith, K. H.; Monge-Marcet, A.; Ferreira, D. S.; Rodríguez, R. P.; Alonso, M.; Rodríguez-Cabello, J. C.; Reis, R. L.; Sagués, F.; Botto, L.; Bitton, R.; Azevedo, H. S.; Mata, A., Co-assembly, spatiotemporal control and morphogenesis of a hybrid protein–peptide system. *Nat. Chem.* **2015,** *7*, 897-904.
10. Freeman, R.; Han, M.; Álvarez, Z.; Lewis, J. A.; Wester, J. R.; Stephanopoulos, N.; McClendon, M. T.; Lynsky, C.; Godbe, J. M.; Sangji, H.; Luijten, E.; Stupp, S. I., Reversible self-assembly of superstructured networks. *Science* **2018,** *362*, 808-813.
11. Kumar, M.; Ing, N. L.; Narang, V.; Wijerathne, N. K.; Hochbaum, A. I.; Ulijn, R. V., Amino-acid-encoded biocatalytic self-assembly enables the formation of transient conducting nanostructures. *Nat. Chem.* **2018,** *10*, 696-703.
12. Boekhoven, J.; Hendriksen, W. E.; Koper, G. J. M.; Eelkema, R.; van Esch, J. H., Transient assembly of active materials fueled by a chemical reaction. *Science* **2015,** *349*, 1075-1079.
13. Tena-Solsona, M.; Rieß, B.; Grötsch, R. K.; Löhrer, F. C.; Wanzke, C.; Käsdorf, B.; Bausch, A. R.; Müller-Buschbaum, P.; Lieleg, O.; Boekhoven, J., Non-equilibrium dissipative supramolecular materials with a tunable lifetime. *Nat. Commun.* **2017,** *8*, 15895.
14. Sorrenti, A.; Leira-Iglesias, J.; Sato, A.; Hermans, T. M., Non-equilibrium steady states in supramolecular polymerization. *Nat. Commun.* **2017,** *8*, 15899.
15. Afrose, S. P.; Bal, S.; Chatterjee, A.; Das, K.; Das, D., Designed Negative Feedback from Transiently Formed Catalytic Nanostructures. *Angew. Chem. Int. Ed.* **2019,** *58*, 15783-15787.
16. Debnath, S.; Roy, S.; Ulijn, R. V., Peptide Nanofibers with Dynamic Instability through Nonequilibrium Biocatalytic Assembly. *J. Am. Chem. Soc.* **2013,** *135*, 16789-16792.
17. te Brinke, E.; Groen, J.; Herrmann, A.; Heus, H. A.; Rivas, G.; Spruijt, E.; Huck, W. T. S., Dissipative adaptation in driven self-assembly leading to self-dividing fibrils. *Nat. Nanotechnol.* **2018,** *13*, 849-855.
18. Gao, Y.; Shi, J.; Yuan, D.; Xu, B., Imaging enzyme-triggered self-assembly of small molecules inside live cells. *Nat. Commun.* **2012,** *3*, 1033.
19. Feng, Z.; Wang, H.; Wang, F.; Oh, Y.; Berciu, C.; Cui, Q.; Egelman, E. H.; Xu, B., Artificial Intracellular Filaments. *Cell Rep. Phys. Sci.* **2020,** *1*, 100085.
20. Liang, Y.; Lynn, D. G.; Berland, K. M., Direct Observation of Nucleation and Growth in Amyloid Self-Assembly. *J. Am. Chem. Soc.* **2010,** *132*, 6306-6308.

21. Wang, H.; Feng, Z.; Del Signore, S. J.; Rodal, A. A.; Xu, B., Active Probes for Imaging Membrane Dynamics of Live Cells with High Spatial and Temporal Resolution over Extended Time Scales and Areas. *J. Am. Chem. Soc.* **2018,** *140*, 3505-3509.
22. Sai, H.; Lau, G. C.; Dannenhoffer, A. J.; Chin, S. M.; Đorđević, L.; Stupp, S. I., Imaging Supramolecular Morphogenesis with Confocal Laser Scanning Microscopy at Elevated Temperatures. *Nano Lett.* **2020**.
23. Sarkar, A.; Dhiman, S.; Chalishazar, A.; George, S. J., Visualization of Stereoselective Supramolecular Polymers by Chirality-Controlled Energy Transfer. *Angew. Chem. Int. Ed.* **2017,** *56*, 13767-13771.
24. Parent, L. R.; Bakalis, E.; Ramírez-Hernández, A.; Kammeyer, J. K.; Park, C.; de Pablo, J.; Zerbetto, F.; Patterson, J. P.; Gianneschi, N. C., Directly Observing Micelle Fusion and Growth in Solution by Liquid-Cell Transmission Electron Microscopy. *J. Am. Chem. Soc.* **2017,** *139*, 17140-17151.
25. Marchello, G.; De Pace, C.; Duro-Castano, A.; Battaglia, G.; Ruiz-Perez, L., End-to-end image analysis pipeline for liquid-phase electron microscopy. *J. Microsc.* **2020,** *279*, 242-248.
26. Müller, D. J.; Dufrêne, Y. F., Atomic force microscopy as a multifunctional molecular toolbox in nanobiotechnology. *Nat. Nanotechnol.* **2008,** *3*, 261-269.
27. Pujals, S.; Feiner-Gracia, N.; Delcanale, P.; Voets, I.; Albertazzi, L., Super-resolution microscopy as a powerful tool to study complex synthetic materials. *Nat. Rev. Chem.* **2019,** *3*, 68-84.
28. Albertazzi, L.; van der Zwaag, D.; Leenders, C. M. A.; Fitzner, R.; van der Hofstad, R. W.; Meijer, E. W., Probing Exchange Pathways in One-Dimensional Aggregates with Super-Resolution Microscopy. *Science* **2014,** *344*, 491.
29. da Silva, R. M. P.; van der Zwaag, D.; Albertazzi, L.; Lee, S. S.; Meijer, E. W.; Stupp, S. I., Super-resolution microscopy reveals structural diversity in molecular exchange among peptide amphiphile nanofibres. *Nat. Commun.* **2016,** *7*, 11561.
30. Chien, M.-P.; Carlini, A. S.; Hu, D.; Barback, C. V.; Rush, A. M.; Hall, D. J.; Orr, G.; Gianneschi, N. C., Enzyme-Directed Assembly of Nanoparticles in Tumors Monitored by In Vivo Whole Animal Imaging and ex Vivo Super-Resolution Fluorescence Imaging. *J. Am. Chem. Soc.* **2013,** *135*, 18710-18713.
31. Fuentes, E.; Boháčová, K.; Fuentes-Caparrós, A. M.; Schweins, R.; Draper, E. R.; Adams, D. J.; Pujals, S.; Albertazzi, L., PAINT-ing Fluorenylmethoxycarbonyl (Fmoc)-Diphenylalanine Hydrogels. *Chem. Eur. J.* **2020,** *26*, 9869-9873.
32. Hell, S. W.; Wichmann, J., Breaking the diffraction resolution limit by stimulated emission: stimulated-emission-depletion fluorescence microscopy. *Opt. Lett.* **1994,** *19*, 780-782.
33. Blom, H.; Widengren, J., Stimulated Emission Depletion Microscopy. *Chem. Rev.* **2017,** *117*, 7377-7427.
34. Tian, X.; De Pace, C.; Ruiz-Perez, L.; Chen, B.; Su, R.; Zhang, M.; Zhang, R.; Zhang, Q.; Wang, Q.; Zhou, H.; Wu, J.; Zhang, Z.; Tian, Y.; Battaglia, G., A Cyclometalated Iridium (III) Complex as a Microtubule Probe for Correlative Super-Resolution Fluorescence and Electron Microscopy. *Adv. Mater.* **2020**, doi: 10.1002/adma.202003901.
35. Kumar, M.; Sementa, D.; Narang, V.; Riedo, E.; Ulijn, R. V., Self-Assembly Propensity Dictates Lifetimes in Transient Naphthalimide–Dipeptide Nanofibers. *Chem. Eur. J.* **2020,** *26*, 8372-8376.
36. Onogi, S.; Shigemitsu, H.; Yoshii, T.; Tanida, T.; Ikeda, M.; Kubota, R.; Hamachi, I., In Situ real-time imaging of self-sorted supramolecular nanofibres. *Nat. Chem.* **2016,** *8*, 743-752.

37. Quinn, M. K.; Gnan, N.; James, S.; Ninarello, A.; Sciortino, F.; Zaccarelli, E.; McManus, J. J., How fluorescent labelling alters the solution behaviour of proteins. *Phys. Chem. Chem. Phys.* **2015,** *17*, 31177-31187.
38. Noel, S.; Liberelle, B.; Robitaille, L.; De Crescenzo, G., Quantification of Primary Amine Groups Available for Subsequent Biofunctionalization of Polymer Surfaces. *Bioconjugate Chem.* **2011,** *22*, 1690-1699.
39. Bieser, A. M.; Tiller, J. C., Surface-induced hydrogelation. *Chem. Commun.* **2005**, 3942-3944.
40. Liu, X.; Kumar, M.; Calo, A.; Albisetti, E.; Zheng, X.; Manning, K. B.; Elacqua, E.; Weck, M.; Ulijn, R. V.; Riedo, E., Sub-10 nm Resolution Patterning of Pockets for Enzyme Immobilization with Independent Density and Quasi-3D Topography Control. *ACS Appl. Mater. Interfaces* **2019,** *11*, 41780-41790.
41. Liu, X.; Kumar, M.; Calo', A.; Albisetti, E.; Zheng, X.; Manning, K. B.; Elacqua, E.; Weck, M.; Ulijn, R. V.; Riedo, E., High-throughput protein nanopatterning. *Faraday Discuss.* **2019,** *219*, 33-43.
42. Beater, S.; Holzmeister, P.; Pibiri, E.; Lalkens, B.; Tinnefeld, P., Choosing dyes for cw-STED nanoscopy using self-assembled nanorulers. *Phys. chem. chem. phys.* **2014,** *16*, 6990-6996.
43. Schreiber, C. L.; Smith, B. D., Molecular conjugation using non-covalent click chemistry. *Nat. Rev. Chem.* **2019,** *3*, 393-400.
44. Raeburn, J.; Mendoza-Cuenca, C.; Cattoz, B. N.; Little, M. A.; Terry, A. E.; Zamith Cardoso, A.; Griffiths, P. C.; Adams, D. J., The effect of solvent choice on the gelation and final hydrogel properties of Fmoc–diphenylalanine. *Soft Matter* **2015,** *11*, 927-935.
45. Reches, M.; Gazit, E., Casting Metal Nanowires Within Discrete Self-Assembled Peptide Nanotubes. *Science* **2003,** *300*, 625-627.
46. Howes, P. D.; Chandrawati, R.; Stevens, M. M., Colloidal nanoparticles as advanced biological sensors. *Science* **2014,** *346*, 1247390.
47. Acuna, G. P.; Bucher, M.; Stein, I. H.; Steinhauer, C.; Kuzyk, A.; Holzmeister, P.; Schreiber, R.; Moroz, A.; Stefani, F. D.; Liedl, T.; Simmel, F. C.; Tinnefeld, P., Distance Dependence of Single-Fluorophore Quenching by Gold Nanoparticles Studied on DNA Origami. *ACS Nano* **2012,** *6*, 3189-3195.
48. Kandela, I. K.; Albrecht, R. M., Fluorescence Quenching by Colloidal Heavy Metals Nanoparticles: Implications for Correlative Fluorescence and Electron Microscopy Studies. *Scanning* **2007,** *29*, 152-161.
49. Yao, Q.; Wang, C.; Fu, M.; Dai, L.; Li, J.; Gao, Y., Dynamic Detection of Active Enzyme Instructed Supramolecular Assemblies In Situ via Super-Resolution Microscopy. *ACS Nano* **2020,** *14*, 4882-4889.
50. Zhang, M.; Li, M.; Zhang, W.; Han, Y.; Zhang, Y.-H., Simple and efficient delivery of cell-impermeable organic fluorescent probes into live cells for live-cell superresolution imaging. *Light Sci. Appl.* **2019,** *8*, 73.

Table of contents